Improvement of Weldability of 1 GPa Grade Twin-Induced Plasticity Steel

A study was conducted related to improving weldability of 1 GPa grade twin-induced plasticity steel using MFDC constant power control welding

BY J. YU, D. CHOI, AND S. RHEE

ABSTRACT

Applications of high-strength steel to car bodies with higher than 1 GPa grade tensile strength have dramatically increased. Twin-induced plasticity (TWIP) steel maintains high strength and secure high ductility, featuring a high content of Mn. In spite of these advantages, the resistance spot weldability is poor. To improve the weldability, conventional AC and MFDC resistance spot welding, and other various types of joint technology have been required and developed. In this work, MFDC constant power control (CPC) welding was applied to improve the weldability of 1 GPa grade TWIP steel, and the welding characteristics were analyzed. To investigate the fundamental weldability of TWIP steel, tensile shear strength, suitable welding range, and welding signal were analyzed. Compared to MFDC constant current control (CCC) welding, CPC welding has the advantage of reducing expulsion at the early stage of the welding process; therefore, it is possible to apply higher heat input to the weld. As a result, it was found that larger nugget size and higher tensile shear strength were obtained in CPC welding than CCC welding. To compare the characteristics of these two welding methods, welding signals were analyzed and high-speed images were used for observing the difference in the nugget growth mechanism. Furthermore, this work evaluated the adaptability of CPC welding according to electrode force changes and coating conditions.

Introduction

In response to the deterioration of the global environment, strict regulations of fuel efficiency to reduce CO_2 emissions have been enforced. In particular, corporate average fuel efficiency (CAFE) standards suggest regulations that affect the fuel efficiency of automobiles, automobile sales, price, and fuel consumption (Ref. 1). The large size of automobiles, the addition of reinforcing parts for safety, and an increase in electronics for the convenience of drivers have increased the weight of car bodies. Under these conditions, the automobile industry has been developing lightweight vehicle technology to solve the problem, especially concentrating on reducing weight with the application of high-strength steel (HSS) (Ref. 2).

Over the last several years, the application of HSS sheet to automobiles for the purposes of increasing collision safety and reducing weight has been expanded. Also, it was reported that the rate of adoption of HSS per automobile stood at more than 50% (Refs. 3, 4). Recently, high-strength 980 ~ 1470 MPa grade hot-stamping steel, is being applied to car bodies (Ref. 2). Although the application of HSS is limited to bumpers, door beams, and the main structural members of automobiles, the adoption rate of HSS is expected to increase (Ref. 3). Steel sheet for automobiles requires both high strength and good formability. However, it is generally known that as the strength of a material increases, the formability decreases. In contrast, when the formability improves, the strength decreases. The relatively poor formability of HSS leads to the limitations of its application to the car body. Conventional use of HSS for automobiles is categorized into dual-phase (DP) steel, complex-phase (CP) steel, and transformation-induced plasticity (TRIP) steel. Maintaining a 15 ~ 25% range of elongation, these DP and TRIP steels satisfy a 600 ~ 1000 MPa range for ultimate tensile strength (UTS) (Ref. 5). To meet the needs for improved formability, the scope of the study has been extended to austenitic Fe-Mn-C alloys. As a result, twin-induced plasticity (TWIP) steel, which shows 60% elongation over an 800 MPa tensile strength was developed (Ref. 6). For welding of TWIP steel, the welding characteristics are different from the conventional HSSs such as DP and CP steel.

To apply lightweight metals such as HSS and aluminum alloy, proper welding and joining technologies are required. Resistance spot welding is the leading joining technology in sheet metal fabrication including the automobile assembly process. As the metals used in car bodies change to lightweight metals, the demand for advanced RSW technology is expected to increase. In particular, the poor resistance spot weldability issue arises when HSS is applied to car bodies and, as a result, a solution is required to solve the problem. In the case of RSW of HSS, a narrow suitable welding range and low toughness caused by brittle welds are the worst problems. Because the high content of alloying elements causes an increase in the resistivity of base metals, the lower boundary of current of suitable welding range relatively shifts to lower range compared to low-carbon steel. Also, at the early stage of the RSW process, the high resistance of the base metal causes excessive heat energy input and, as a result, the current in which expulsion occurs decreases compared to low-carbon steel. Since its decrement is larger than that of the lower boundary of current, the suitable welding range becomes narrow. To reduce the expulsion and widen the suitable welding range, high electrode force, low welding current, and long welding times are required (Refs. 7, 8).

Nowadays, the weldability issue of HSS, welding characteristics of TWIP steel, and development of welding technology to improve weldability have been intensively studied. Saha (Ref. 9) studied

J. YU and S. RHEE (srhee@hanyang.ac.kr) *are with the Department of Mechanical Engineering, Hanyang University, Seoul, Korea. D. CHOI is with Product Application Center, POSCO, Korea.*

KEYWORDS

TWIP980
High Strength Steel
MFDC Constant Power Control Welding
Weldability
Welding Signals

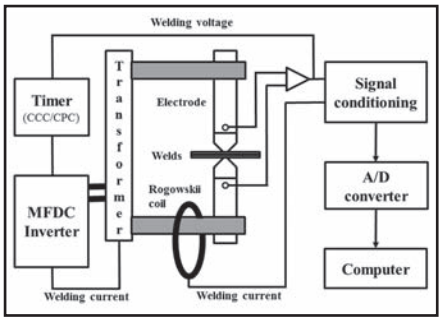

Fig. 1 — Schematic of welding signal monitoring system.

Table 1 — Chemical Composition of TWIP980 (mass%)

	C	Mn	Etc.	Fe
TWIP980	0.60	18.0	Al	Bal.

Table 2 — Welding Conditions

Items	Conditions
Welding machine	Air-pressure control type MFDC 130 kVA
Cooling temperature	20°C
Cooling rate	6 L/min
Electrode fore (kN)	2.0 / 3.0 / 5.0
Hold time (ms)	300
Welding time (ms)	150 / 200 / 250 / 300 / 350

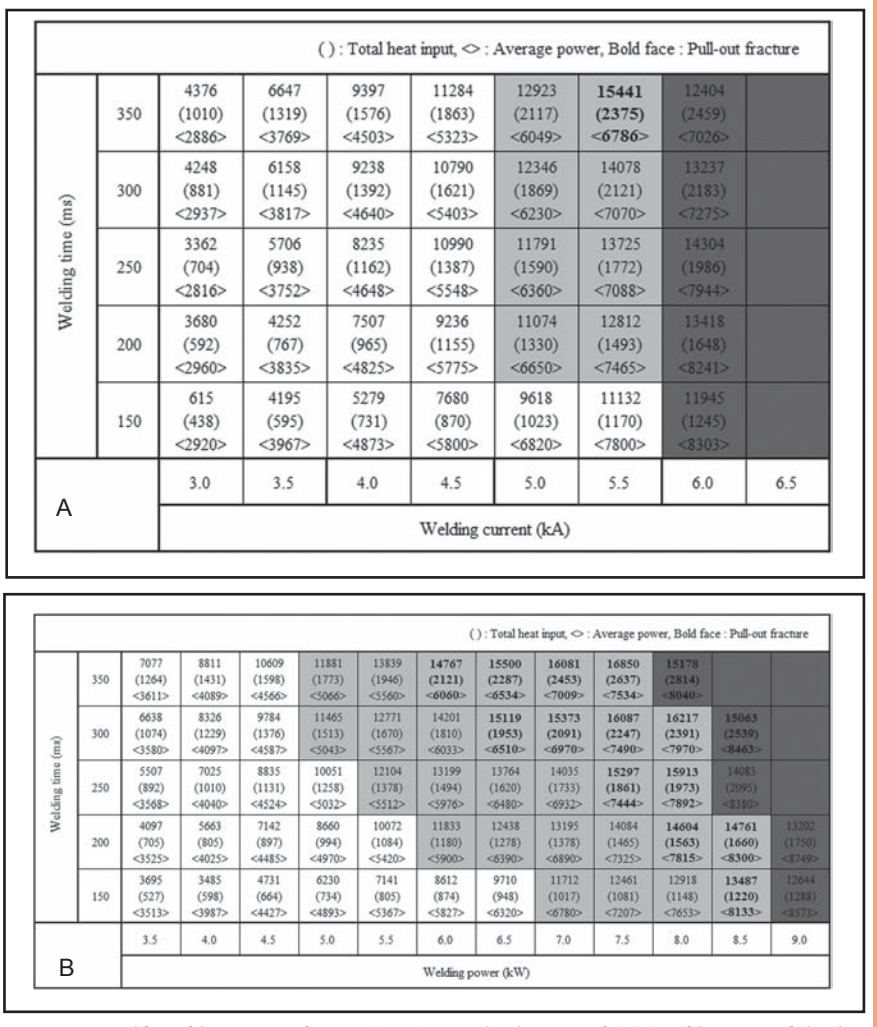

Fig. 2 — Suitable welding range of TWIP980. A — Lobe diagram of CCC welding; B — lobe diagram of CPC welding.

resistance spot weldability of 1 GPa TWIP steel for automobile applications, especially focusing on the metallurgical and mechanical properties of the weld. Yu (Ref. 10) evaluated the weldability of TWIP980 steel by using the medium-frequency direct current (MFDC) constant current control (CCC) RSW process, and comparatively analyzed the RSW characteristics of TWIP980 steel with DP980 steel, which has the same strength, thickness, and surface treatment. Nevertheless, few studies have been conducted on methods to improve the weldability of TWIP steel. Tumuluru (Ref. 11) analyzed the correlation between the failure mode of resistance spot welds of DP steel, weld diameter, and hardness of the weld. Brown (Ref. 12) evaluated weldability by analyzing the welding signals of alternating current (AC) and MFDC RSW, and thus revealed that the suitable welding range of MFDC was larger than that of AC RSW. Alfaro (Ref. 13) compared the nugget growth mechanisms of AC and MFDC RSW by using high-speed filming, and discovered that MFDC RSW secured a more uniform nugget in a short welding time than did AC RSW. By using a nonlinear feedback linearization technique, Kim (Ref. 14) controlled the welding power of the RSW system and conducted computer simulations to illustrate the performance of the controller. However, the RSW process primarily applied for sheet metal was MFDC CCC welding, which showed its technical limitations in the case of the application of welding HSS. In that aspect, the MFDC constant power control (CPC) method was developed to solve the limitation problems and apply it to actual manufacturing process. Therefore, more studies on the differences between CPC welding characteristics and the conventional welding characteristics need to be conducted.

In this work, MFDC CCC and CPC welding were applied to 1 GPa grade TWIP steel in order to compare the characteristics of each welding process. A lobe diagram was used to compare suitable welding ranges. For comparison analysis on each welding mechanism, welding signals and high-speed images were used. Furthermore, to investigate the adaptability of CPC welding to the changes in the welding condition, comparison tests on CCC and CPC welding were conducted with regard to change in electrode force and on galvanized (GI) coated steel as well.

Materials

The material used in this work was cold-rolled TWIP steel sheet of 980 MPa grade. The chemical composition of TWIP980 is indicated in Table 1. TWIP980 is composed of 18% Mn, 0.6% C, and Al as a minor alloying element. The test steel sheet is 1.4 mm thick; uncoated and GI-coated steel were used as well. To analyze the fundamental welding characteristics of the test material and the mechanisms of CCC and CPC welding, uncoated TWIP980 was used. The coating amount of the GI-coated TWIP980 was 60 g/m^2, which was used to evaluate the adaptability of CPC welding to a coating layer.

Equipment and Experimental Procedure

In this experiment, a MFDC pedestal-type RSW system with 130 kVA capacity

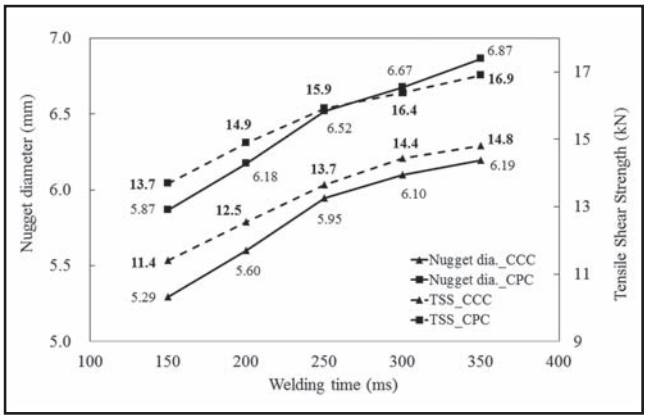

Fig. 3 — Maximum tensile shear strength and nugget diameter of TWIP980.

was developed as shown in Fig. 1. The developed welding system was a MFDC RSW machine with 1 kHz switching frequency. By controlling pulse width modulation (PMW), two modes, CCC welding and CPC welding are possible in the same welding machine. The welding timer receives the welding current feedback from the transformer (a Bosch Rexroth PGS6130), and welding voltage feedback from both electrode tips. With the use of the developed welding system, it is possible to maintain the additional experimental conditions including electrode force, electrode alignment, welding gun, and a cooling condition equally in CCC and CPC modes. Aside from the welding timer, a Rogowski coil (DC flex, PEM Corp.) for current measurement was installed to measure the welding signals that were actually given to the weld, and both tips of the electrode were clipped to measure the voltage. By using an analog-to-digital converter (a National Instruments NI9229), analog current and voltage were measured at the same time with a rate of 50,000 samples per second per channel. Since the control frequency of the MFDC RSW machine used was 1 kHz and the sampling rate was 50 kHz, 25 data per 0.5 ms were used for resistance and power calculation. Digitized welding voltage and current in root mean square (RMS) value were computed per 0.5 ms. Finally, resistance and power were calculated with Equations 1 and 2 as follows:

$$r(t) = v(t)/i(t) \quad (1)$$

$$p(t) = v(t)/i(t) \quad (2)$$

where, $i(t)$ is the RMS value of the welding current, $v(t)$ is the RMS value of the welding voltage, $r(t)$ is the resistance, and $p(t)$ is the power (Ref. 15).

Cu-Cr dome-type electrodes having a tip diameter of 6 mm and a tip radius of 40 mm were used, and the electrode tips were conditioned by making 50 welds prior to the experiment (Refs. 16, 17). Specimen size was 125 mm × 40 mm. The welding experiments were conducted on two sheets of the same type of TWIP980. Details of the experimental conditions are described in Table 2, and other details of the testing methodology can be found in the ISO standard (Ref. 18).

Results and Discussion

Suitable Welding Range of TWIP980

To evaluate the weldability of TWIP980, a suitable welding range of test material was used. Generally, a suitable welding range is indicated through a lobe diagram using welding current, welding time, and electrode force. Also, to evaluate the welding characteristics of CCC and CPC welding, a suitable welding range was drawn through a lobe diagram of welding current and welding time while the electrode force was fixed at 3.0 kN. The lower boundary of the suitable range was related to the acceptable tensile shear strength, and the upper boundary was dependent on occurrence of expulsion. The acceptable tensile strength was set as 11091 N (Ref. 19). Figure 2 shows the lobe diagram of TWIP980 in the case of both CCC and CPC welding. In Fig. 2A, the vertical axis stands for welding time and the horizontal axis for welding current. The white range in the diagram represents the conditions where tensile shear strength is insufficient, the gray area is for suitable welding conditions and the dark area represents the welding conditions considered as defective welding by expulsion. Welding conditions written in boldface type represent pull-out fractures during the shear tension test, and the other conditions are interfacial fractures. To compare CCC and CPC welding, tensile shear strength and total heat input to the weld as well as average welding power were recorded. Total heat input was calculated with Equation 3, and average power was calculated by dividing total heat input with welding time. In each welding condition, three values indicate tensile shear strength, total heat input, and average welding power. The top value stands for tensile shear strength, the value in the blank in the middle for total heat input; and the value in the angle blank on the bottom for average welding power. Each unit of the values is N, J, and W. In Fig. 2B, the vertical axis stands for welding time, and the horizontal axis for welding power. It is a quasi-lobe diagram to compare with the general lobe diagram of CCC welding.

$$Q_{total} = \eta \cdot \int i^2(t) \cdot r(t) \cdot dt = \eta \cdot \int i(t) \cdot v(t) \cdot dt = \eta \cdot \int p(t) \cdot dt \quad (3)$$

where, Q is heat, η is welding thermal efficiency, $i(t)$ is welding current, $r(t)$ is electrical resistance of the weld, $v(t)$ is welding voltage, $p(t)$ is welding power, and t is the time the welding current is applied to the test material (Ref. 10).

As shown in Fig. 2A, the welding current range for CCC welding is 5.0 ~ 5.5 kA, total heat input range is 1330 ~ 2375 J, and average welding power range is 6049 ~ 7465 W in the suitable welding range. In contrast, in the case of CPC welding in Fig. 2B, the range of total heat input is 1017 ~ 2637 J, and the range of average welding power is 5043 ~ 8300 W in the suitable welding range. Therefore, compared to CCC welding, it was found that total heat input to the weld and the upper and lower boundary of average welding power range expanded farther in CPC welding. Also, owing to higher heat input on the weld than CCC welding, it is considered that a larger weld is formed, and thereby higher tensile shear strength is secured. A larger weld and higher tensile shear strength led to an increase in welding conditions that caused pull-out fractures. In the case of TWIP980 sheet with the thickness of 1.4 mm, it is considered that tensile shear strength, a boundary between interfacial fracture and pull-out fracture in shear tension test, stands at approximately 14000 N.

To investigate the relation between tensile shear strength and nugget diameter, nugget diameter was measured through the cross-sectional image of the weld in all welding conditions just before the occurrence of expulsion, which is shown in Fig. 2. In other words, the maximum tensile shear strength and nugget diameter that can be secured according to the welding time were measured and compared. The weld cross section was etched with Nital (5% HNO_3; 95% ethanol) and then magnified 40× with an optical microscope for observation. Figure 3 shows the relation between the tensile shear strength of the weld and its nugget diameter. Since the nugget diameter is proportional to the tensile shear strength and CPC welding is able to give higher heat input to the weld than does CCC welding, the nugget diameter was larger; therefore, the maximum tensile shear strength appeared to be higher. In addition, in both CCC and CPC welding, the longer the welding time, the higher the total heat input is to the weld. As a result, it was found that both nugget diameter and tensile shear strength increased.

To find the reason for the difference in total heat input between CCC and CPC

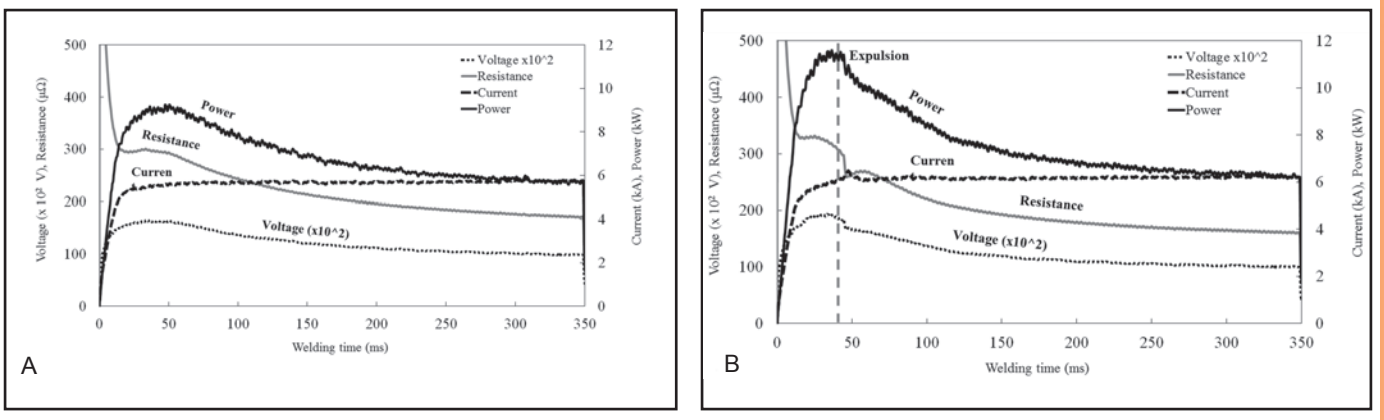

Fig. 4 — Welding signals of CCC welding. A — Without expulsion (3.0 kN/5.5 kA/350 ms); B —with expulsion (3.0 kN/6.0 kA/350 ms).

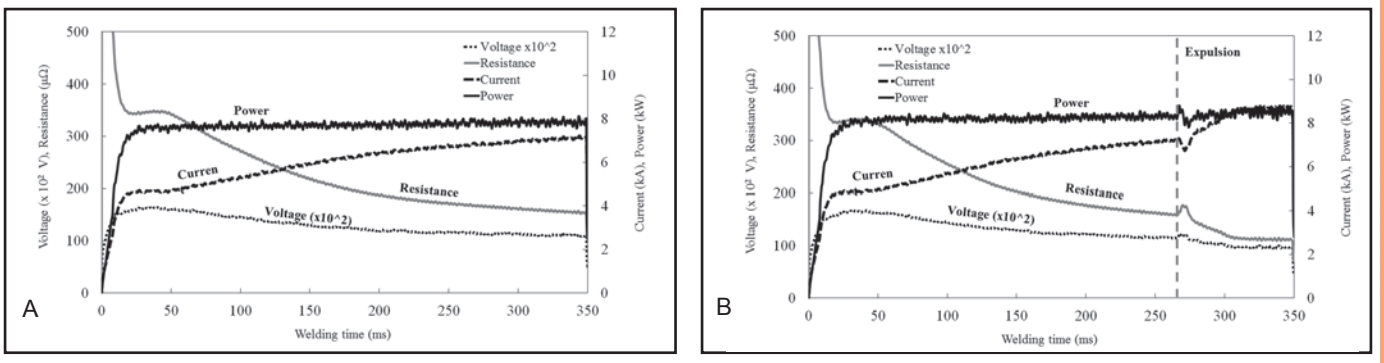

Fig. 5 — Welding signals of CPC welding. A —Without expulsion (3.0 kN/7.5 kW/350 ms); B — with expulsion (3.0 kN/8.0 kW/350 ms).

welding, welding signals for each welding mode were measured. Figure 4 shows welding signals of CCC welding for welding conditions without and with expulsion. The total heat input shown in Fig. 4A is 2375 J, and it is the maximum heat input among suitable welding conditions. In the case of CCC welding, since the welding current is constant, as shown in Equations 2 and 3, its power and resistance are determined by the welding voltage. Since heat input to the weld is an area under the welding power curve, high heat input is given at the early stage of a welding process, and then is gradually reduced. In the case of TWIP980, as welding current more than 6.0 kA is applied, excessive heat in the weld is generated as shown in Fig. 4B. Due to the excessive heat input, expulsion occurs at an early stage in the process. For this reason, in the case of CCC welding, the upper boundary of a suitable welding range has a limitation in expansion to the higher welding current range. Also, in Fig. 4B, the resistance, voltage, and power decline rapidly when an expulsion occurs because molten metal expels out of the weld because of excessive heat input. Figure 5 presents welding signals of CPC welding in welding conditions without and with expulsion. The total heat input at the time shown in Fig. 5A is 2637 J, which is the maximum heat input for the suitable welding range. Since CPC welding controls welding power constantly, welding current changes in response to the change in weld resistance unlike in CCC welding. In other words, to maintain the constant power as shown in Fig. 5A, relatively low current is applied at the early stage of a welding process depending on the changes in resistance. Then, to compensate for the change in resistance that is on the decrease at the latter stage of the welding process, welding current increases gradually. Since constant power is supplied over the entire process, the heat energy is constantly applied to the weld. In

Table 3 — Tensile Shear Strength according to Electrode Force Change

Constant Current Welding			Constant Power Welding		
Force (kN)	Tensile Shear Strength (N)	Average Tensile Shear Strength (N)	Force (kN)	Tensile Shear Strength(N)	Average Tensile Shear Strength(N)
2.0	12752 13173 12070	12665 (Expulsion)	2.0	13850 14080 13888	13939
3.0	12783 12797 12848	12809	3.0	12674 12833 12816	12774
5.0	10650 10898 10953	10834 (Insufficient TSS)	5.0	12390 12655 12065	12370

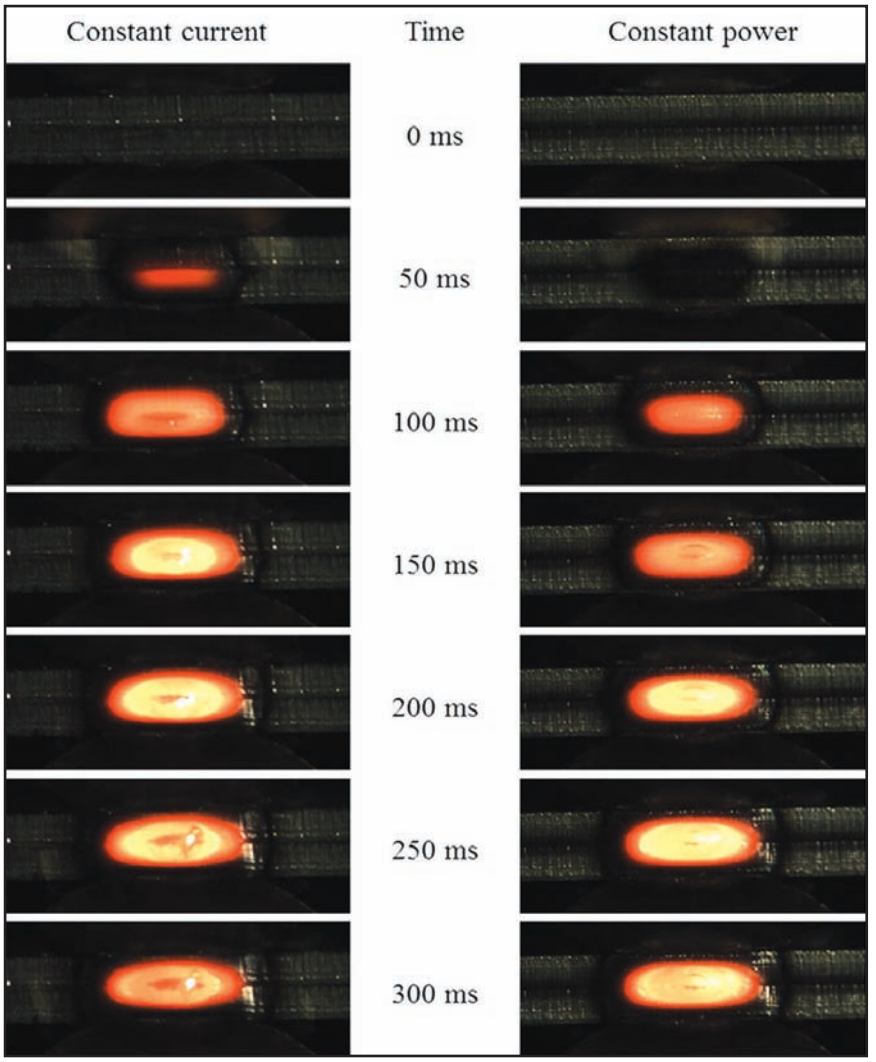

Fig. 6 — Nugget growth images for CCC and CPC welding.

Table 4 — Tensile Shear Strength of GI-Coated TWIP980 Steel

Welding Condition	Tensil Shear Strength (N)	Average Tensile Shear Strength (N)
CCC 3.0 kN	11870 12477 12693	12347
CPC 3.0 kN	13296 13149 12738	13061

this aspect, since CPC welding effectively reduces expulsions caused by excessive heat input at the early stage of a welding process, it is possible to increase the total heat energy that can be given to the weld. Therefore, as shown in Fig. 2B, it is possible to secure a higher tensile shear strength and a wider suitable welding range. Regarding an aspect of expulsion occurrence shown in Fig. 5B, expulsion in CCC welding occurs at the early stage of the welding process, whereas expulsion in CPC welding occurs at a relatively later stage of the welding process. Of course, expulsion in CPC welding can also occur at an early stage of the welding process when welding is conducted with excessively high power.

Nugget Growth Mechanisms of CCC and CPC Welding

To compare the difference in the nugget growth mechanism between CCC and CPC welding, high-speed filming was used. There is previous research using high-speed film photography (Ref. 13), and generally the welding process in progress is observed in the state that an electrode cap tip and a specimen are cut in half. However, in that state, the boundary condition of a weld becomes different from the boundary condition of actual welding. Therefore, it is difficult to quantitatively configure welding parameters, such as electrode force, welding current, and power. Accordingly, to qualitatively compare the difference between the nugget growth mechanism of CCC welding and that of CPC welding, a trial-and-error method was used to configure the welding parameters. The maximum current and power conditions where melting metal is not expelled in the weld were set using a trial-and-error method, and thus each welding condition of CCC and CPC welding was, respectively, 1.0 kN, 300 ms, 2.5 kA, and 1.0 kN, 300 ms, 2.0 kW. The camera speed for observation was set to 2000 frames per second.

Figure 6 shows a high-speed image of CCC and CPC welding at 50 ms intervals. In the case of CCC welding, nugget formation was faster than in CPC welding; however, after 200 ms, nugget growth remained still, and at 300 ms, the nugget started to cool. On the other hand, in the case of CPC welding, although nugget formation was slower than with CCC welding, the nugget consistently grew until 300 ms. Finally, it was observed that the CPC welding secured the same or larger nugget size than CCC welding. The cause for the difference in the nugget growth mechanism can be inferred by the difference in the welding power profiles shown in Figs. 4 and 5. In the case of CCC welding, since high welding power is applied to the weld early in the welding process, the nugget forms quickly. However, the welding power constantly decreases. As a result, it is considered that the nugget growth stands still. In the case of CPC welding, since constant welding power is applied to the weld over the entire welding process, nugget growth is relatively slow but keeps growing.

Welding Characteristic on Electrode Force and Coating

To test the adaptability according to the changes in electrode force and the surface treatment (GI coating), each characteristic of CCC and CPC welding was compared. In the condition that electrode force is 3.0 kN and welding time is 350 ms, the total heat input was equally set as a criterion of test conditions for both CCC and CPC welding. The test condition was set about 2120 J as total heat input in Fig. 2. Therefore, the welding conditions were set as 5.0 kA, 350 ms for CCC welding, and 6.0 kW, 350 ms for CPC welding. To evaluate the adaptability of CPC welding for the changes in electrode force, these welding conditions were used for conducting tests on electrode force with

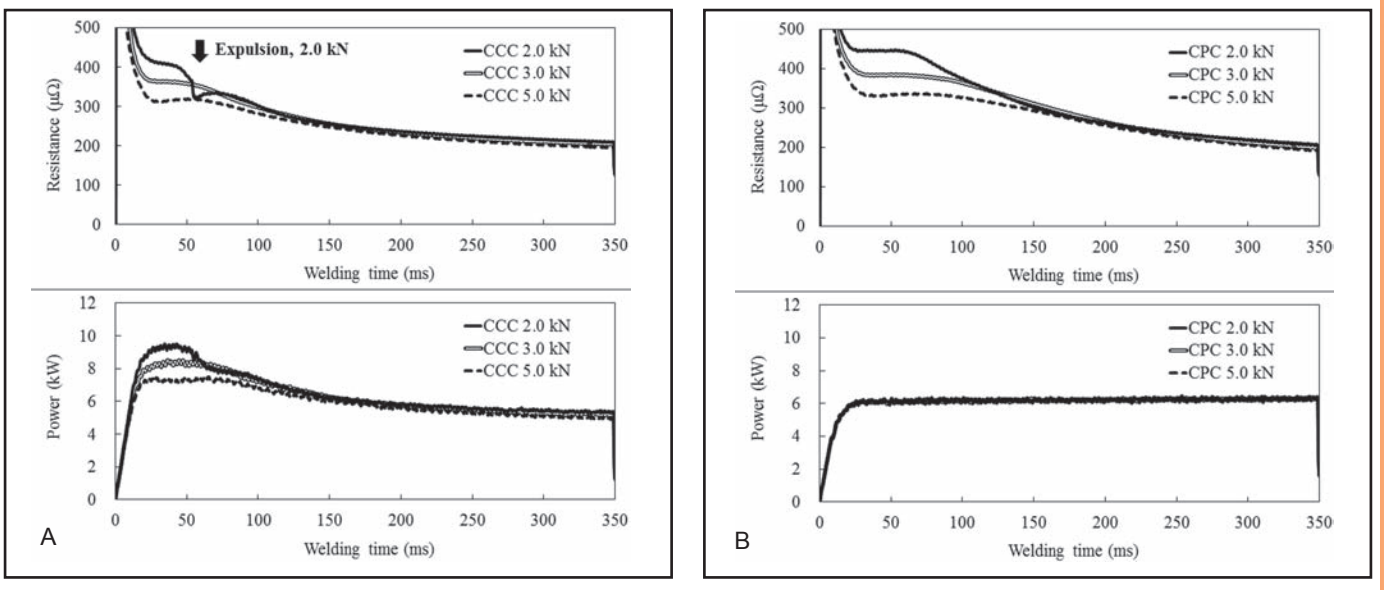

Fig. 7 — Resistance and power signals according to the electrode force. A — CCC welding; B — CPC welding.

three levels, 2.0, 3.0, and 5.0 kN. Table 3 shows the results of the tests on electrode force with three levels. In each condition, three tests were repeatedly conducted. In the case of CPC welding, it satisfies acceptable tensile shear strength for all force conditions. In contrast, in the case of CCC welding, with an electrode force of 2.0 kN, expulsion occurred in all three repeated tests due to an increase in dynamic resistance. Also, with an electrode force of 5.0 kN, it failed to secure the acceptable tensile shear strength in three repeated tests due to the lack of heat input caused by a reduction in dynamic resistance. Therefore, regarding the changes in electrode force, it can be concluded that the adaptability of CPC welding is better than that of CCC welding.

Figure 7 shows each dynamic resistance and power curve for CCC and CPC welding in each condition that electrode force is 2.0, 3.0, and 5.0 kN. In both CCC and CPC welding, the lower the electrode force, the higher the resistance. As shown in Fig. 7A, in the case of CCC welding, since the welding current is constant, the electrode force is lower, and the welding power is higher. That is, as the electrode force gets lower, the total heat input (an area under the power curve) applied to the weld increases. Therefore, in the 2.0 kN condition, excessive heat energy is applied to the weld early in the welding process, and thereby expulsion occurs. In the 5.0 kN condition, since the lack of total heat energy causes insufficient nugget formation, acceptable tensile shear strength is not secured. While in the case of CPC welding, since equal heat energy is applied to the weld under the three levels of electrode force, as shown in Fig. 7B, acceptable tensile shear strength can be obtained in all force conditions. That is because, as shown in Fig. 8, CPC welding compensates for the resistance change caused by a force condition by changing the welding current. The lower the resistance, the higher the current, and vice versa. The result indicates that, regarding the changes in electrode force, the adaptability of CPC welding is better than that of CCC welding.

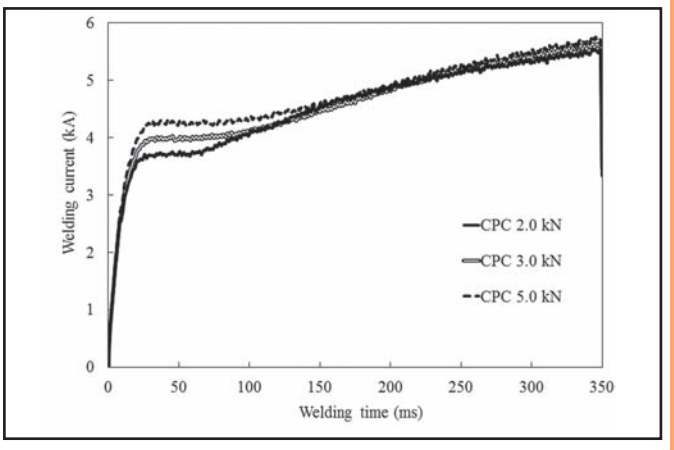

Fig. 8 — Welding current profiles of CPC welding under three electrode forces.

To evaluate the adaptability of CPC welding to the GI coating layer of the test material, welding of GI-coated TWIP980 steel sheet with the same thickness of 1.4 mm was conducted. Table 4 shows the results of CCC and CPC welding of GI-coated TWIP980 steel. In both CCC and CPC welding, no expulsion was found, and acceptable tensile shear strength was secured. The tensile shear strength of CPC welding was about 700 N higher than that of CCC welding. That is because the total heat input of CCC welding decreases due to the GI coating layer. However, CPC welding compensates for the resistance drop caused by the GI coating layer, and thus applies equal total heat input as the uncoated TWIP980 steel.

Figure 9 shows the dynamic resistance and power curve of both uncoated and GI-coated TWIP980 welding. In the case of the GI-coated steel, resistance of each CCC and CPC weld decreased. As shown in Fig. 9A, in the case of CCC welding, welding current is constant and welding power decreases due to the resistance drop caused by the GI coating layer. Since total heat energy is an area of power curve, it decreases due to the effect of the GI coating layer. As a result, the tensile shear strength of the coated steel is lower than that of the uncoated steel. However, in the case of CPC welding, since equal heat energy is given to the weld regardless of coating treatment, as shown in Fig. 9B, CPC welding secures higher tensile shear strength than CCC welding. As shown in Fig. 10, because CPC welding compensates for the resistance change caused by the GI coating layer, the welding current changes. The lower the resistance, the higher the current, and vice versa. Like the test result of adaptability to electrode force changes, it is considered that, regarding GI coating, the adaptability of CPC welding is better than that of CCC welding.

Conclusions

This work applied MFDC CPC welding, and evaluated weldability through comparison with conventional MFDC CCC

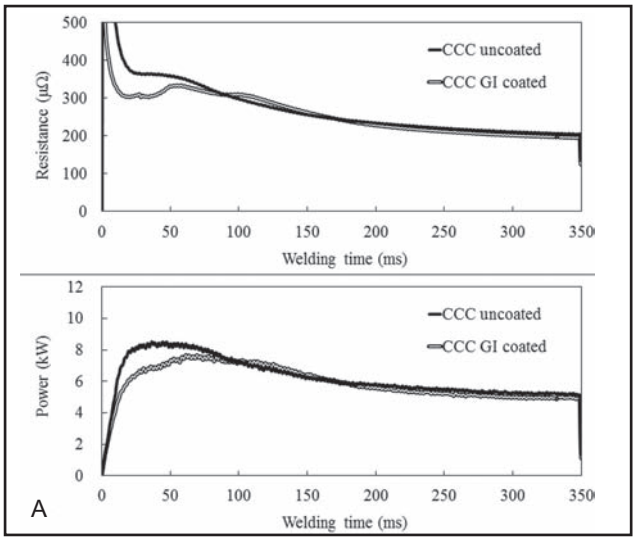

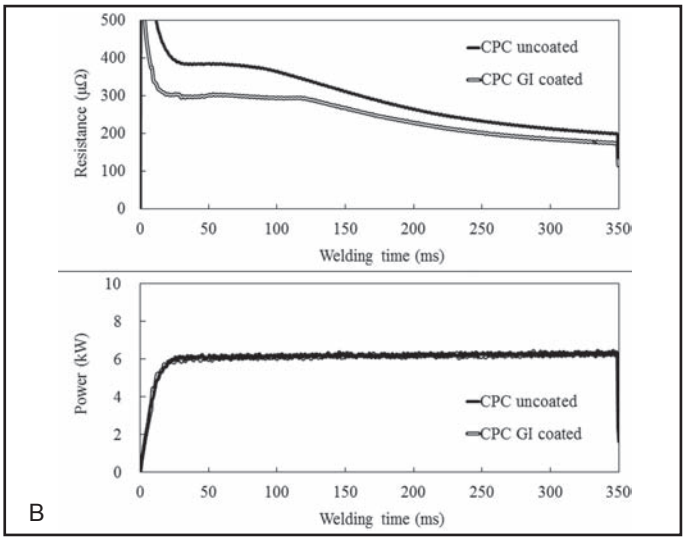

Fig. 9 — Resistance and power signals of uncoated and GI-coated TWIP steels. A — CCC welding; B — CPC welding.

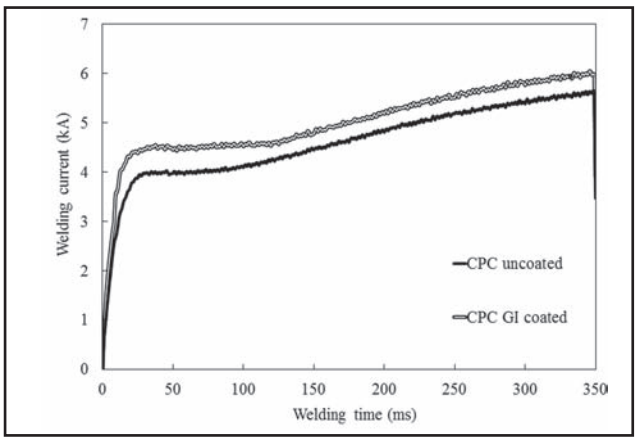

Fig. 10 — Welding current profiles of CPC welding of uncoated and GI-coated TWIP steels.

welding, to improve resistance spot weldability of 1 GPa grade TWIP steel. The following conclusions were drawn from the investigation on the weldability of the MFDC constant power welding and constant current welding to 1 GPa grade TWIP steel:

1. By evaluating fundamental weldability, this work obtained the suitable welding range of both CCC and CPC welding for TWIP980 steel. Furthermore, it was found that the suitable welding range for CPC welding was larger than that of CCC welding with regard to total heat input. Also, it was found that nugget diameter was proportional to tensile shear strength.

2. Constant power control welding reduced expulsion because it prevents excessive heat input to the weld durging the early stage of the process. Therefore, the suitable welding range for CPC welding was expanded.

3. Due to the heat input profile (i.e., a different power profile) of CPC being different from CCC welding, there are different nugget growth mechanisms between CPC welding and conventional welding (i.e., CCC welding).

4. Constant power control welding showed better weldability in the case of coated steel and for different electrode force conditions.

Acknowledgments

This work was supported by the National Research Foundation of Korea (NRF) grant funded by the Korea government (MEST) (No. 2012-0005415).

References

1. Goldberg, P. K. 1998. The effects of the corporate average fuel efficiency standards in the U.S. *Journal of Industrial Economics* 46(1): 1–33.

2. Oikawa, H., Murayama, G., Sakiyama, T., Takahashi, Y., and Ishikawa, T. 2007. Resistance spot weldability of high strength steel (HSS) sheets for automobiles. *Nippon Steel Technical Report* (95): 39–45.

3. Nonaka, T., Taniguchi, H., Goto, K., and Yamazaki, K. 2003. Development of ultrahigh-strength cold-rolled steel sheets for automotive use. *Nippon Steel Technical Report* (88): 13–15.

4. Nielsen, C. V., Friis, K. S., Zhang, W., and Bay, N. 2011. Three-sheet spot welding of advanced high-strength steels. *Welding Journal* 90 (2): 32-s to 40-s.

5. Bracke, L., Verbeken, K., Kestens, L., and Penning, J. 2009. Microstructure and texture evolution during cold rolling and annealing of a high-Mn TWIP steel. *Acta Materialia* 57(5): 1512–1524.

6. Barbier, D., Gey, N., Allain, S., Bozzolo, N., and Humbert, M. 2009. Analysis of the tensile behavior of a TWIP steel based on the texture and microstructure evolutions. *Materials Science and Engineering A* 500(1-2): 196–206.

7. Chuko, W. L., and Gould, J. E. 2002. Development of appropriate resistance spot welding practice for transformation-hardened steels. *Welding Journal* 81(1): 1-s to 7-s.

8. Radakovic, D. J., and Tumuluru, M. 2008. Predicting resistance spot weld failure modes in shear tension tests of advanced high-strength automotive steels. *Welding Journal* 87(4): 96-s to 105-s.

9. Saha, D. C., Han, S., Chin, K. G., Choi, I., and Park, Y.-D. 2012. Weldability evaluation and microstructure analysis of resistance-spot-welded high-Mn steel in automotive application. *Steel Research International* 83(4): 352–57.

10. Yu, J., Shim, J., and Rhee, S. 2012. Characteristics of resistance spot welding for 1 GPa grade twin induced plasticity steel. *Materials Transactions* 53(11): 2011–2018.

11. Tumuluru, M. D. 2006. Resistance spot welding of coated high-strength dual-phase steels. *Welding Journal* 85(8): 31–37.

12. Brown, B. M. 1987. Comparison of AC and DC resistance welding of automotive steels. *Welding Journal* 66(l): 18–23.

13. Alfaro, S. C. A., Vargas, J. E., Wolff, M. A., and Vilarinho, L. O. 2007. Comparison between AC and MF-DC resistance spot welding by using high speed filming. *Journal of Achievements in Materials and Manufacturing Engineering* 24(1): 333–339.

14. Jun, S., Kim, G., Kim, J., and Won, C. 1997. Power control of resistance spot welding system with high dynamic performance. *Proc. 23rd Ind. Electron. Control Instrum. Conf.* eds. Anon, pp. 845–849. IEEE Comp. Soc.

15. Cho, Y., and Rhee, S. 2002. Primary circuit dynamic resistance monitoring and its application to quality estimation during resistance spot welding. *Welding Journal* 81(6): 104-s to 111-s.

16. International Standard, ISO18278-2 — Resistance welding — Weldability — Part 2: Alternative procedures for the assessment of sheet steels for spot welding, 2004.

17. International Standard, ISO14327 — *Resistance welding — Procedures for determining the weldability lobe for resistance spot, projection and seam welding*, 2004.

18. British Standard, BE EN ISO14273 — *Specimen dimensions and procedure for shear testing resistance spot, seam and embossed projection welds*, 2001.

19. AWS D8.1M:2007, *Specification for Automotive Weld Quality Resistance Spot Welding of Steel*. Miami, Fla.: American Welding Society.